Enhanced Luminescent Stability through Particle Interactions in Silicon Nanocrystal Aggregates

Joseph B. Miller,[†,∥] Naveen Dandu,[†] Kirill A. Velizhanin,[§] Rebecca J. Anthony,[‡,¶] Uwe R. Kortshagen,[‡] Daniel M. Kroll,[†] Svetlana Kilina,[†] and Erik K. Hobbie*[,†]

[†]North Dakota State University, Fargo, North Dakota 58108, United States, [§]Theoretical Division, Los Alamos National Laboratory, Los Alamos, New Mexico 87545, United States, and [‡]University of Minnesota, Minneapolis, Minnesota 55455, United States. [∥]Present address: Rice University, Houston Texas 77005, United States [¶]Present address: Michigan State University, East Lansing, Michigan 48824, United States

ABSTRACT Close-packed assemblies of ligand-passivated colloidal nanocrystals can exhibit enhanced photoluminescent stability, but the origin of this effect is unclear. Here, we use experiment, simulation, and *ab initio* computation to examine the influence of interparticle interactions on the photoluminescent stability of silicon nanocrystal aggregates. The time-dependent photoluminescence emitted by structures ranging in size from a single quantum dot to agglomerates of more than a thousand is compared with Monte Carlo simulations of noninteracting ensembles using measured single-particle blinking data as input. In contrast to the behavior typically exhibited by the metal chalcogenides, the measured photoluminescent stability shows an enhancement with respect to the noninteracting scenario with increasing aggregate size. We model this behavior using time-dependent density functional theory calculations of energy transfer between neighboring nanocrystals as a function of nanocrystal size, separation, and the presence of charge and/or surface-passivation defects. Our results suggest that rapid exciton transfer from "bright" nanocrystals to surface trap states in nearest-neighbors can efficiently fill such traps and enhance the stability of emission by promoting the radiative recombination of slowly diffusing excited electrons.

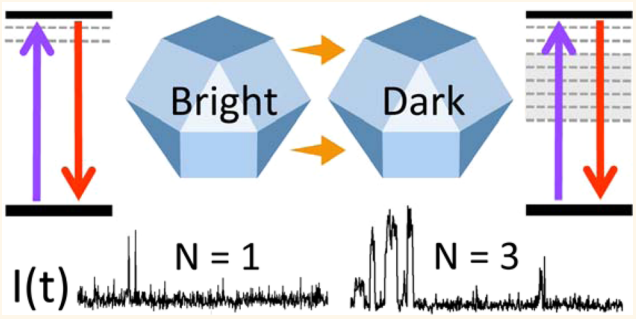

KEYWORDS: silicon nanocrystals · fluorescence intermittency · nanocrystal interactions · energy transfer

The tunable emission enabled by quantum confinement imparts semiconductor nanocrystals with a unique band gap photoluminescence (PL) that shows considerable promise for fluorescent tagging and sensing applications.[1,2] By far, the most widely and deeply studied materials in this regard have been the metal chalcogenides such as CdSe, which offer excellent quantum yield, broad color access, fast lifetime, narrow line width, and improved photoluminescent stability over conventional fluorophores.[3] Although such materials are commercially available, easily endowed with specific biochemical functionality, and are presently being used with a remarkable degree of effectiveness, an element of uncertainty regarding the potential toxicity of the metal chalcogenides[4−6] has generated a significant amount of activity directed at finding nontoxic earth-abundant alternatives. In this regard, nanocrystalline silicon has emerged as a material of considerable current interest.

Silicon nanocrystals (SiNCs) synthesized through a variety of plasma-assisted[7−11] or solution-based[12−17] chemistries exhibit tunable PL across the visible to the near-infrared.[16−20] Once imparted with colloidal stability through ligand passivation or other surface treatment, SiNCs can be separated by size to yield monodisperse colloidal suspensions.[21−24] In terms of PL, the potential utility of these materials has already been demonstrated for a range of bioimaging[25−27] and responsive polymer nanocomposite[28−30] applications. Nonetheless, there are a number of unresolved questions related to the role of surface states,[31] the interplay of quantum confinement and the indirect band gap of silicon,[32] and the impact of particle interactions on PL.[33,34] In terms of the latter, an intriguing trait recently reported for nanocrystal "solids" assembled from colloidal

* Address correspondence to erik.hobbie@ndsu.edu.

Received for review May 4, 2015 and accepted September 8, 2015.

Published online September 08, 2015
10.1021/acsnano.5b02676

SiNCs is an ensemble brightening under continuous excitation, where the emission and PL lifetime exhibit a temporal increase instead of the usual photobleaching.[21] Similar behavior has also been observed in the metal chalcogenides, where it has been attributed to dark-state passivation mediated by mobile photoexcited electrons.[35] In a much broader view, energy transfer from nanocrystals to polymers, dye molecules, or other acceptors is a topic of considerable current interest.[36−39]

A fundamental understanding of such phenomena must start with the smallest distinct element: the emission from an individual nanocrystal. Like all fluorophores, semiconductor nanocrystals exhibit fluorescence intermittency or "blinking", whereby the PL randomly switches between bright (*on*) and dark (*off*) states.[40−46] The *off* state of a semiconductor nanocrystal has commonly been associated with charge/ionization states and subsequent Auger-assisted recombination. However, recent insight from controlled electrochemical studies on CdSe suggests two distinct blinking mechanisms: a charging/decharging of the nanocrystal core, where low PL correlates with shorter lifetime, and a second mechanism in which electron-accepting surface states intercept "hot" electrons before they can radiatively relax into the core.[42] These are delineated A-type and B-type blinking, respectively. Interestingly, both mechanisms can be electrochemically suppressed by the application of an appropriate potential.[42] An even higher level of complexity is suggested by the recent observation that the emission time trace of a single nanocrystal is not just binary, but can be multileveled in a manner that reflects the potentially complex energy landscape of surface trap states.[47] A significant amount of information related to nanocrystal blinking and photostability is thus contained in the time-dependent emission.[48−55]

Here, we use experiment, simulation and *ab initio* computation to examine the influence of interparticle interactions on the photoluminescent stability of SiNC aggregates. To the best of our knowledge, this is the first in-depth study of the blinking behavior of ligand-stabilized colloidal SiNCs, either as individuals or as a collective. The time-dependent PL emitted by structures ranging in size from an isolated SiNC up to dense assemblies containing thousands of nanocrystals is measured at varied excitation power and particle-size homogeneity. Measurements as a function of aggregate size are compared with Monte Carlo (MC) simulations of noninteracting ensembles that employ measured single-particle blinking data as input. In contrast to the behavior typically observed for CdSe, we find a significant stabilizing effect with respect to the noninteracting scenario, which we model using density functional theory (DFT) calculations of energy transfer between neighboring nanocrystals as a function of SiNC size, separation, and the presence of charge and/or surface defects. Our results suggest that rapid exciton transfer from "bright" nanocrystals to trap states in nearest-neighbors can efficiently fill such traps and enhance the PL stability by promoting the radiative relaxation of slowly diffusing excited electrons.

RESULTS AND DISCUSSION

We consider both a parent material (denoted AP) and a monodisperse fraction (denoted F) of comparable mean size (4 nm) as determined by transmission electron microscopy (TEM). Both have peak PL emission near 750 nm and a particle size in the vicinity of the exciton Bohr radius of silicon.[21] Blinking as a function of time was measured over long intervals with large ensembles for each sample type (F vs AP) at both low (LP, 140 W/cm^2) and high (HP, 5000 W/cm^2) power under 473 nm CW excitation. Although a single emitter can be identified through photon antibunching in the PL intensity autocorrelation function,[38] we seek to discriminate intensity as a function of aggregate size over very long time scales and thus benefit from a different approach that relies on real-space verification of the size of the emitter. Some typical results are shown in Figure 1. The smallest resolvable feature in atomic force microscopy (AFM) was identified to be a single SiNC by using successively smaller AFM scans while deconvolving the contribution of the tip profile from the height signal. Details are given in the Supporting Information.

Typical blinking sequences are shown in Figure 1d for a range of emitter size. For an accessible description of the *on*/*off* statistics in light of the complex emission dynamics anticipated for an aggregate, we first render these time traces into binary *on*/*off* sequences in the usual way through a threshold intensity set to exclude background noise. Examples can be found in Figure 1d,e. The equivalent binary waveform then yields *on* and *off* statistics, as shown in Figure 2 for the *on* times under a variety of conditions. Additional distributions are shown in the Supporting Information. The distributions are mostly power laws, with a small number of truncated power laws of the form $p(t) \propto t^{-\alpha} \exp(-t/\tau)$. A table of the relevant fitting parameters is given in the Supporting Information (Tables S1 and S2). The exponent α decreases with increasing N and varies between 1.5 and 3, where the larger end is likely influenced by uncertainties associated with the cutoff. For single-nanocrystal emission, the nature of such power laws has been shown to depend on the precise choice of threshold and binning.[56,57] Although this is not a critical issue for the brighter aggregates, we nonetheless avoid relying exclusively on these fitting parameters to draw meaningful conclusions. In Figure 2a,b, the dashed curve for $N = 16$ is the behavior obtained by summing 16 single-dot ($N = 1$) time traces, which is well below the measured *on*-time distribution for $N = 16$.

The various moments of these distributions (Figure 3) are revealing and typically scale in a power-law fashion

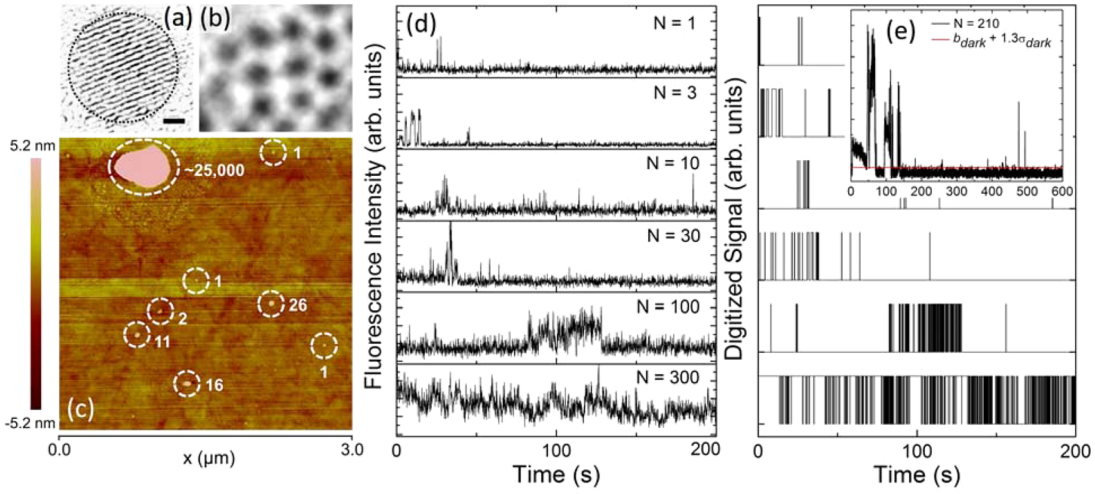

Figure 1. (a) TEM image of a single SiNC (1 nm scale). (b) TEM image of a packed assembly of monodisperse 4 nm diameter SiNCs. (c) AFM scan showing SiNCs clusters of varied size, including a large cluster used as a coordinate reference point. (d) Typical time-dependent PL traces collected for varied *N*. (e) Binary fluorescent signals from panel (d) based on an intensity threshold as depicted in the inset for $N \approx 200$.

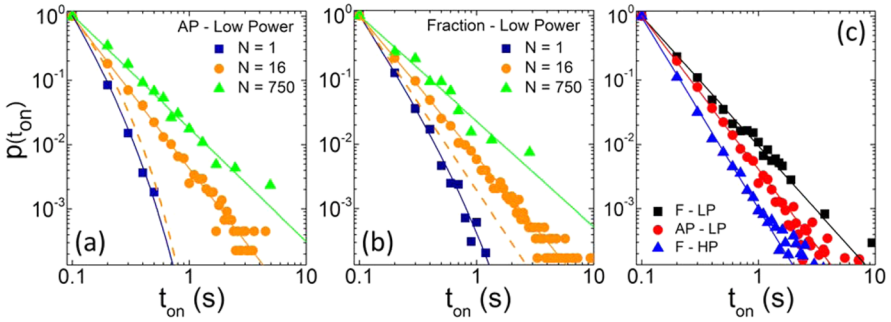

Figure 2. (a) *On* time statistics for a collection of as-produced (AP) SiNC aggregates of size $N = 1$, 16, and 750 at low excitation power and (b) a similar plot obtained for a monodisperse fraction (F). The dashed curves in (a) and (b) are the $N = 16$ distributions tabulated from 16 independent $N = 1$ blinking traces. (c) *On* time statistics for the monodisperse fraction and AP material at low excitation power and the fraction at high power, where the data include all *N*. Distributions are normalized to $p = 1$ at $t_{on} = 0.1$ s.

as N^{β}, where a table of the exponents can be found in the Supporting Information (Table S3) along with additional quantities (Figure S6, Supporting Information). The general trends are better stability and longer *on* time at lower excitation power and lower size disparity. Focusing on the fraction at low power, we can again compare the measured behavior with that anticipated for *N* independent single emitters (green curves, Figure 3) which now includes both MC simulations (dashed green) and the behavior obtained by summing *N* measured single SiNC time sequences (solid green). The MC simulations are indeed consistent with the integrated $N = 1$ experimental results, but both differ from the measured behavior, as can be seen by comparing the green curves (no interactions) with the black curves (measured) in Figure 3. This difference is most meaningful for the average *on* time (Figure 3a) since the maximal values will depend on the particular measured $N = 1$ traces chosen for size integration.

With the exception of Figure 3a, the exact values of the exponents in the power-law trends do not vary drastically with excitation power or size homogeneity, but there are large differences in the amplitude of the effect. The behavior at higher excitation power reflects the fact that we are operating in a regime of very few emitters compared to the number of incident photons, and more emitters are thus being driven into dark states at higher photon flux through rapid and repeated excitation. In terms of interaction effects, the data in Figures 2 and 3 suggest that aggregates are more stable than the same number of individuals regardless of size distribution. On top of this, however, the data suggest that such interaction effects are enhanced for narrower size distributions (Figure 3a).

As detailed in Figure 4, the same trends can be seen in the autocorrelation function of the time-dependent emission: $c(t) = \langle I(t')I(t' + t)\rangle / \langle I(t')I(t')\rangle$, where the brackets denote an average over t'. This is determined directly from the background-corrected PL intensity and is thus independent of *on*/*off* binning or binarization.[58] For each *N* in Figure 4, the data represent an average over many features of identical (for $N = 1$ and small *N*) or

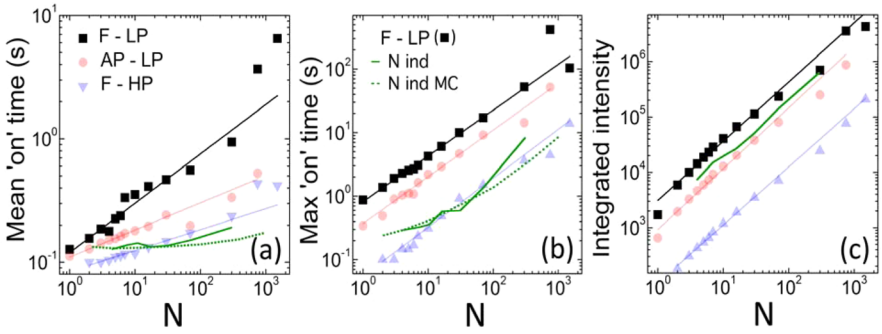

Figure 3. (a) The mean *on* time, (b) the maximum *on* time, and (c) the integrated intensity as a function *N*. In each panel, the green curves are the equivalent quantity computed from the appropriate number of individual (*N* = 1) SiNCs for the fraction at low power (F-LP) based on both measurement (solid) and MC simulation (dashed).

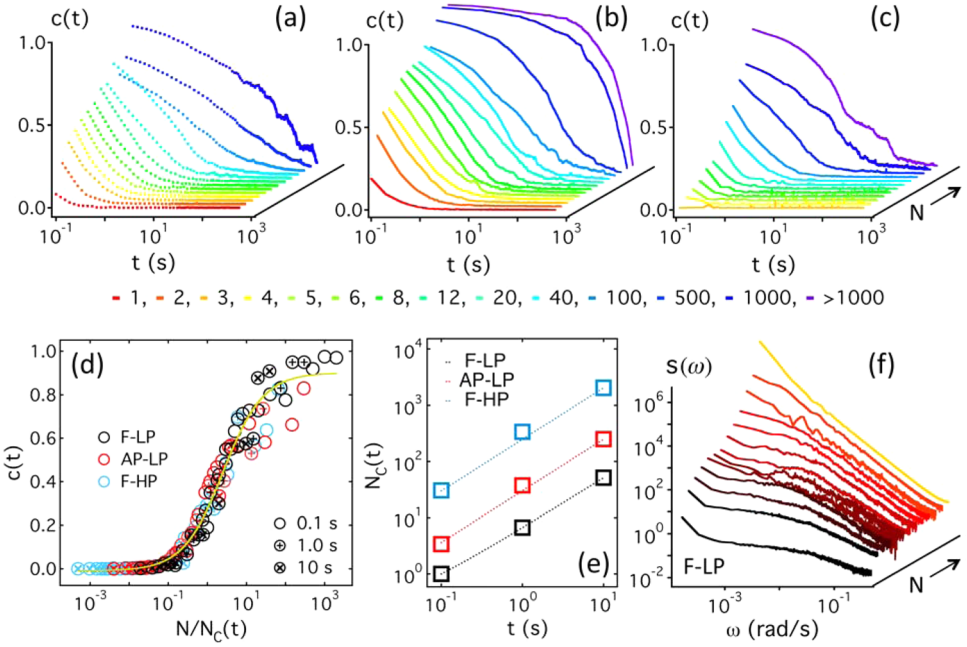

Figure 4. Fluorescence autocorrelation function *c*(*t*) as a function of *N* for (a) the as-produced (AP) material under low excitation power, (b) the fraction (F) under low excitation power, and (c) the fraction under high excitation power. The color legend for *N* is shown below the graphs. (d) Scaling plot of the *N*-dependence of *c*(*t*) for each scenario at the indicated times (0.1, 1.0, and 10 s) in terms of a single time-dependent scaling parameter N_c. (e) The time dependence of N_c for each scenario and (f) the *N* dependence of *S*(ω) for the F-LP data shown in panel (b).

comparable mean (for much larger *N*) size. For small *N*, *c*(*t*) decays to zero with increasing time because there is no long-*t* correlation in the intensity. For large *N*, the abrupt late-*t* cutoff reflects the finite size of the sampling interval, and we thus limit our quantitative analysis to $t < 10-10^2$ s. Figure 4a,b suggests a correlation time that increases with increasing aggregate size and decreasing power, which we quantify by first considering projections of *c*(*t*) onto the *N* axis at varied time. All such projections can be scaled onto a single master curve by defining a time-dependent critical size, $N_c(t)$, as shown in Figure 4d,e. All scenarios show the same power-law dependence; $N_c \propto t^{\gamma}$ with $0.9 < \gamma < 1$. What differs is the proportionality constant, which increases by a factor of 3 from F-LP to AP-LP and by nearly a factor of 40 from F-LP to F-HP. Physically, N_c is the minimum size exhibiting emission stability over a time interval *t*. For long time intervals, only clusters much larger than N_c exhibit stable emission. This is evident in the Fourier transform of *c*(*t*) [the spectral power density, *S*(ω)], which exhibits a low-frequency divergence for the largest *N* (Figure 4f, F-LP). The linearity of N_c as a function of time is also evident in logarithmic intensity plots of *c*(*t*) in the *t*-*N* plane, as shown in Figure 5a−c.

The results of Figures 4e and 5 are revealing. The spin-coating process creates assemblies that tend to be coplanar (Figure 1c), so there is a simple average relationship between cluster size, *N*, and cluster length scale, *R*, with $N \propto R^2$. Figure 4e shows that N_c is nearly linear in time, which implies $R_c^2 \approx 4Dt$ with a diffusion coefficient, *D*, given by the proportionality constant in Figure 4e. Specifically, we find $D \approx 10$ nm^2/s (F-LP), 45 nm^2/s (AP-LP), and 370 nm^2/s (F-HP). The increase in

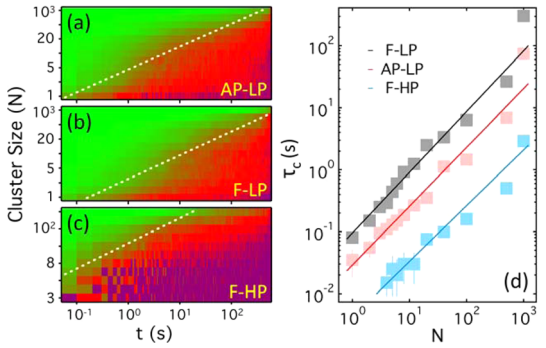

Figure 5. Log intensity plots of $c(t)$ in the plane of size and time for (a) AP-LP, (b) F-LP, and (c) F-HP. The lines indicate linear time dependence, where deviations from this trend are due to a distribution of sizes that is not perfectly logarithmic. (d) Correlation time vs size with power-law fits that are close to linear (exponents from 0.9 to 0.98). Data for $\tau_c < 100$ ms are interpolated from spline fits down to $c(0) = 1$.

D between F-LP and F-HP (~35×) mirrors the increase in excitation power, implying that the diffusion coefficient is proportional to fluence. Because $c(t)$ obtained from a sum of N single (N = 1) emitters does not show this enhanced correlation (Figure S7, Supporting Information), we further infer that $N_c(t)$ is determined by SiNC interactions. Diffusion-controlled processes have previously been identified in the blinking of CdSe nanocrystals,[43] but to our knowledge this is the first time they have been reported for silicon. Here, we note that the scaling in Figure 4d implies an analogous scaling in terms of $t/\tau_c(N)$, where $\tau_c \propto N/D \propto R^2/D$ is a correlation time. Fits of τ_c (the time required to decay to 1/e) as a function of N are shown in Figure 5d. The physical interpretation of projecting the data in this manner is that aggregates in an *on* state at $t = 0$ are still likely to be *on* at $t = \tau_c$, where τ_c increases nearly linearly with size. A final piece of insight comes from the supporting movies (Movies 1 and 2), which show that aggregates turn *off* abruptly (faster than ~100 ms). This implies that the temporal decay of $c(t)$ at fixed N arises from a statistical superposition of different *on* times and not from a gradual *on*−*off* transition.

Taken collectively, the experimental data reveal some important and surprising trends. First and foremost, SiNC aggregates exhibit enhanced PL stability, regardless of the magnitude of the excitation power or the narrowness of the size distribution. The causal role of defects,[59−61] surface trap states,[62−65] and charge[66−72] in the PL intermittency of quantum dots is well documented, and the logical conclusion is that nearest-neighbor SiNCs "passivate" each other by reducing the collective number of surface trap states available to the ensemble. An attractive way to explain this would be through a transfer scheme in which excitons from a "bright" nanocrystal occupy the trap states of a "dark" neighbor. Second, higher excitation power reduces but does not eliminate this collective trend. The higher the flux of incident photons, the more frequently a given nanocrystal will be excited across the band gap and the more likely the relaxing electron will encounter a trap state, but nearest neighbors still provide a stabilizing effect. Third, size disparity reduces this collective enhancement through disorder in the band gap energy, which has been shown to slow down exciton transport through close-packed lattices.[73]

Although the above ideas are intuitive, they require a computational foundation. Toward this end, we used time-dependent DFT (TD-DFT) to compute inter-SiNC energy-transfer rates for scenarios relevant to the experiments. A DFT-based approach was recently used to study the role of dangling-bond defects in the blinking behavior of individual oxidized SiNCs.[74] These studies confirm the presence of hot-electron traps in oxidized SiNCs, which are important for B-type blinking. While this approach[74] treats an excitation as an unbound electron−hole pair, recent calculations[75] show that excitonic effects are much stronger in SiNCs than in bulk Si, and they cannot be neglected for energy-transfer calculations. In addition, it has been shown[76] that multipolar terms dominate the Coulomb coupling when the distance between nanocrystals is smaller than 2 nm. Our approach to energy transfer thus includes both excitonic effects and multipole terms in the Coulomb integral for the coupling between neighboring SiNCs.

The SiNCs were modeled as Si clusters with a bulk-diamond structure. We consider 29 Si atoms (1.2 nm diameter), 35 Si (1.35 nm diameter), and 66 Si (1.6 nm diameter). Methane ligands were covalently bonded to the surface Si atoms to passivate dangling bonds. The fully passivated structures are denoted F, but we also simulated defective SiNCs by removing a ligand from each of the two nearest 3-coordinated Si atoms (denoted L) and charged structures with ±2 charge introduced on both fully passivated ($F^{2\pm}$) and defective ($L^{2\pm}$) SiNCs. Förster resonant energy transfer (FRET) rates k_{ET} were then calculated between different SiNC donor/acceptor pairs at varied separation based on the DFT transition density matrix. As shown in the top panel of Figure 6a, the band gap under full passivation exhibits quantum confinement. The presence of surface defects and surface charge leads to trap states within the gap (bottom panel, Figure 6a), resulting in the appearance of red-shifted dark and semi-dark optical transitions in the absorption spectra, as shown in the middle panel of Figure 6a. Additional calculations can be found in the Supporting Information. Figure 6b shows the varied structure of the Si_{35} nanocrystal for both the fully passivated scenario (left) and for a charged defect (right, two missing ligands with two surface electrons). The top panel is the structure, and the middle panel shows the natural transition orbital (NTO) for an excited electron and a hole contributing to the lowest-energy optical transition, illustrating an increase in the localization of the

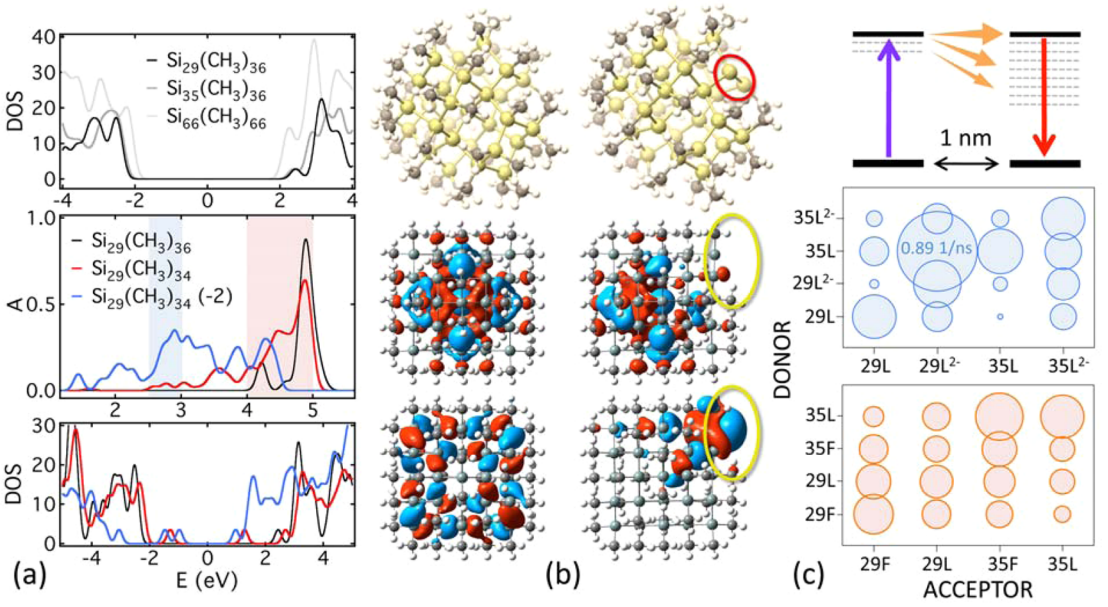

Figure 6. (a) (top) Computed DOS for varied SiNC size; (middle) absorbance for defect-free Si_{29} (black), with two ligands removed (red), and with two missing ligands and −2 charge (blue); (bottom) computed DOS for the scenarios in the middle panel, where energy is the horizontal axis in all three plots. (b) Simulated structures for (left) defect-free Si_{35} and (right) the L^{2-} configuration (two missing ligands + two electrons) (top) and the excited orbital (NTO) for an electron (middle) and hole (bottom). The defect is located in the top right corner. (c) (top) Band diagram for energy transfer from a "bright" SiNC to a "dark" (defective) SiNC and (bottom) area-based bubble charts of k_{ET} for a variety of donor/acceptor pairs at 1 nm separation. The blue data (middle) consider the effect of a missing ligand and charge, while the red data (bottom) consider the effect of only a missing ligand, where the common bubble scale is indicated for the highest rate. Blue/red data are excited at the blue/red region in (a).

electron−hole density around the defect, which decreases the oscillator strength of such transitions. A schematic of the transfer scenario and the computed k_{ET} for a variety of scenarios are shown in Figure 6c. In the middle panel, the excitation is implemented over the optically weak lower energy band, marked by blue in Figure 6a, and present only in charged and defective SiNCs, while in the lower panel the excitation involves the most optically active band, marked by red in Figure 6a.

The energy-transfer rate between neighboring SiNCs decays strongly with distance, while multipole contributions are crucial for separations near 1 nm, particularly when photoexcitation involves optically weak lower energy transitions, with more than an order of magnitude difference in k_{ET} between dipole−dipole and multipole approaches (Supporting Information, Figure S10). At the fixed separation of 1 nm in Figure 6, it depends on two factors: the transition dipole moment of the donor/acceptor and the DOS of the acceptor at the excitation energy of the donor; k_{ET} is maximized when both are optimal. Indeed, these conditions are satisfied when the donor and acceptor have identical structure, as observed in most of the scenarios in Figure 6c (a few exceptions to this rule are discussed in the Supporting Information). This is consistent with the experimental observation of enhanced PL stability in the size-purified fraction and supports the hypothesis of band alignment through band gap homogeneity. The calculated k_{ET} are 2 orders-of-magnitude faster than the radiative recombination rates that we compute from TD-DFT (Supporting Information). Within the DFT framework, energy transfer is thus efficient on the scale of 10 ns, even for states with low oscillator strength (semidark trap states), which provides an additional channel for occupying the lowest-lying dark or semi-dark states. For phonon-induced relaxation, energy transfer thus facilitates the occupation of nonradiative trap states, which would increase the stability of PL from optically bright states associated with the nanocrystal core. This, in turn, would lead to an increase in the average *on* time for densely packed SiNC ensembles, consistent with the experiments.

Previous work on the blinking of isolated nanocrystals suggests significant differences between silicon and CdSe.[48,77−79] In particular, a B-type blinking mechanism in SiNCs has been associated with the activation/deactivation of a nonradiative recombination center associated with dangling surface bonds.[74] Type B blinking arises when "hot" electrons get caught in surface trap states and are unable to recombine with a hole.[42,74] Here, the linear scaling of τ_c with N can be explained by a simple tentative argument that bridges the experiments to the DFT. To identify a characteristic time scale, we model the quantum yield of an aggregate as

$$\Phi \approx \frac{k_R + \zeta k_{ET}}{k_R + k_{NR} + k_{ET}} \quad (1)$$

where k_R is the radiative rate constant, k_{NR} is the nonradiative rate constant, k_{ET} is the rate constant associated

with energy transfer (assumed to be the fastest channel present), and the parameter ζ sets the balance between radiative and nonradiative effects associated with energy transfer. Assuming the slow process of interest resides in the nonradiative channel, the rate of change is $\dot{\Phi} \approx \zeta \dot{k}_{NR}/k_{ET}$.

We further hypothesize that k_{NR} is proportional to the concentration of hot electrons, φ, which is proportional to the excitation power, p. The lower number of nearest-neighbor SiNCs at the aggregate boundary means that energy transfer will be less efficient there, implying that there will be more unoccupied trap states at the edge. Diffusion then implies $\dot{k}_{NR} \propto \partial\varphi/\partial t \propto D_0\varphi/R^2$, where D_0 is a bare diffusion coefficient of hot electrons, which gives $\dot{\Phi} \propto k_{ET}^{-1} D_0\varphi/R^2 \propto k_{ET}^{-1} D_0\varphi/N \propto \tau_c^{-1}$, or $\tau_c \propto N/D_{eff}$ with an effective diffusion coefficient $D_{eff} \propto \varphi D_0/k_{ET} \propto pD_0/k_{ET}$. This increases linearly with power (in agreement with the experiments) and is inversely proportional to k_{ET}. At equal excitation power, the experiments give $D_{AP}/D_F \approx 3$, which would imply $(k_{ET})_F/(k_{ET})_{AP} \approx 3$. This can be compared with the ratio of the average k_{ET} for identical and different sizes in Figure 6c ($\sim$2.2 excluding the 35L-29L^{2-} outlier), where the difference might reflect other variables such as excess ligand in the parent. The magnitude of D (10^{-13} to 10^{-11} cm^2/s) is comparable to the diffusion coefficient of electrons in polyethylene,[80] suggestive of diffusion in the ligand shell, although more work is needed to fully understand this intriguing slow process. The physical picture that emerges is thus the diffusion-controlled accumulation of hot electrons in traps at the boundary, which eventually causes the agglomerate to abruptly turn *off* when exciton transfer can no longer compensate for the increasing number of trapped electrons.

Previous in-depth studies of the PL intermittency from SiNCs have focused on single emitters in noncolloidal structures,[77−79] but the influence of nanocrystal interactions on the blinking of SiNC aggregates has not been previously considered for any type of SiNC. Interaction effects have been investigated for colloidal CdSe quantum dots and nanorods,[81−85] while a handful of other papers have examined energy transfer from a nanocrystal to a dissimilar object, such as a dye molecule,[36,86] graphene,[37] a conjugated polymer,[38] or a nearby surface.[39] In general, such work suggests that interaction effects and/or energy transfer give rise to faster blinking rates or suppressed nanocrystal *on* times, which is the opposite of what we observe here. One exception is the work of Wang et al. on core/double-shell CdSe nanorods,[82] who found enhanced *on* times without any discernible interaction effects in the *off* times. On one level, this suggests that there must be something unique about the double-shell CdSe nanorod structures with respect to other CdSe nanocrystals. More relevant to the point of this study, it suggests that nanocrystal interactions have a clear beneficial effect on the PL stability of colloidal SiNC assemblies.

Finally, we explain the different magnitude of the effect apparent in the mean *on* time (Figure 3a) compared to the integrated intensity (Figure 3c). In simple terms, the mean *on* time is the total *on* time (Figure S6a, Supporting Information) divided by the total number of blinking events in an observation interval. The sublinear N-dependence of the mean *on* time in Figure 3a implies that the number of such blinking events increases with N, but not as fast as the total *on* time. This is intuitive, since the number of such events should increase with the number of emitters. The difference in total *on* time between N and the sum of N individuals is rather modest (Figure S6a, Supporting Information), which implies that the temporal density of blinking events must increase more strongly with N in the noninteracting scenario; N individuals blink more often than an aggregate, or the latter exhibit better PL stability.

The integrated intensity, in contrast, is just the summed intensity of each time frame. This can be trivially coarse-grained to $\sum_j I_j$, where the index j corresponds to a single blinking event and I_j is the total intensity of the event. The integrated intensity is thus proportional to the total number of blinking events multiplied by the average intensity per event, with the data in Figure 3c suggesting that the integrated intensity is proportionally to N for both the interacting and noninteracting scenarios. From the mean *on* time discussed above, however, we know that the number of blinking events increases more strongly with N for the integrated $N = 1$ results, which implies that the total intensity per blinking event increases more slowly. In terms of the N-dependence with and without interactions, the intensity-related quantity that is analogous to mean *on* time is thus the mean total intensity per blink, which is enhanced due to the enhanced stability associated with interactions. We note that the data also suggest that the constant of proportionality in Figure 3c is slightly smaller for the integrated $N = 1$ results, since the difference in amplitude is outside of the uncertainty (a roughly 20% combined uncertainty compared to a 40% difference based on purely linear fits through the origin). This is a much smaller effect, however, that is closer to the resolution limit of the experiments.

CONCLUSIONS

In conclusion, we have used experiment, simulation, and *ab initio* computation to examine the role of interparticle interactions on the PL stability of colloidal SiNC aggregates. In contrast to the behavior typically reported for CdSe, the measured stability as a function of increasing collective size shows an enhancement with respect to the noninteracting scenario. We have modeled this behavior using time-dependent DFT calculations of energy transfer between neighboring nanocrystals in the presence of charge and/or

surface-passivation defects. Our results suggest that rapid energy transfer—or more precisely, exciton transfer[75,87]—from "bright" nanocrystals to "dark" trap states in nearest-neighbors can efficiently fill such trap states and improve the stability of aggregate emission. Although a rigorous theoretical accounting extended to larger SiNC sizes is still needed, this mechanism gives us one possible foundation for a more quantitative explanation of how nanocrystal interactions improve the PL stability of aggregates.

Focusing on the autocorrelation data, our results can be interpreted in terms of a fluence-dependent slow diffusion of hot electrons that is tempered by particle interaction effects. Just as an individual SiNC abruptly transitions to the *off* state when an electron gets caught in a surface trap state, an aggregate abruptly turns *off* when a sufficient number of "hot" electrons have found unoccupied trap states. In our model, these trap states have a higher density at the boundary where the energy-transfer scheme is less efficient. It would thus take longer for this to happen for larger *N*, since it requires the slow diffusion of electrons to the boundary. Modeling these interaction effects using TD-DFT yields predictions that are qualitatively supported by the data.

The results make sense intuitively, given the critical role of surface passivation in the PL of SiNCs. At these excitation powers, we typically observe that a single SiNC is more likely to exhibit short *on* times. Only in the presence of other nanocrystals do these *on* times begin to become appreciable. We suspect that this has something to do with the dried state of the colloidal SiNCs, as we measured the quantum yield of the nanocrystal solutions just prior to these measurements and found the anticipated results.[8−11,21] One possibility is that a lack of solvent in the ligand coating—perhaps coupled to residual surface stress associated with spin coating—causes individual SiNCs to be "darker" under these particular circumstances. In the presence of other nanocrystals, however, it does not appear to be an issue, due presumably to the fast filling of these trap states via energy transfer and subsequent relaxation mechanisms. Our results suggest that this effect could make a substantial contribution to the PL stability of close-packed nanocrystal solids, which will have important implications for any application that seeks to exploit the PL from dense SiNC arrays. The trends reported here also likely represent a foundation for a more precise explanation of the ensemble brightening reported for much larger "bulk" SiNC structures,[21] and quantitatively bridging these two effects will be the objective of future work.

MATERIALS AND METHODS

Plasma-synthesized SiNCs of nominal mean diameter 4 nm were passivated with 1-dodecene as capping ligand to impart solubility in organic solvents[8−11] and separated by size using density-gradient ultracentrifugation in chloroform/*m*-xylene mixtures, as detailed in the Supporting Information.[21−23] Optical measurements were taken under a purified nitrogen atmosphere on a customized inverted microscope using a 473 nm CW laser for excitation and a 60× 1.35 NA oil-immersion objective for imaging. Dilute SiNC solutions were spin-coated on ultraclean quartz slides, and the PL intermittency and background were measured immediately. After initiating excitation, fast transients (comparable to the integration time) were allowed to relax prior to data collection. A schematic of the experiment (Figure S1) and additional details can be found in the Supporting Information, along with typical movies (Movies 1 and 2) of blinking ensembles.

Bright-field images were collected in order to identify large reference aggregates, and a digital grid was constructed based on these landmarks. Using this grid, specific PL signals were then mapped onto SiNC clusters of varied size *N via* high-resolution AFM immediately after optical interrogation. The size of a reference cluster was corrected for spatial resolution and packing effects to get cluster size *N*. Once the blinking behavior for a large number of references had been directly correlated with the independently determined agglomerate size for each sample and excitation power, a linear proportionality relation was established between *N* and the average PL intensity (Figure S2, Supporting Information), and these linear relationships were then used to deduce *N* from the purely optical signals of many thousands of assemblies for each scenario. Details can be found in the Supporting Information.

For DFT, we modeled the SiNCs as clusters of Si atoms in a bulk diamond structure, where computational constraints require that the nanocrystals are smaller than those in the experiments. For surface passivation, 2 or 1 methane groups were covalently bonded to each 2- or 3-coordinated Si, respectively, to mimic experimental SiNC passivation by short alkyl chains. All structures were optimized at the DFT level using the PBE1 hybrid functional and 6-31g* basis set. Linear-response TD-DFT calculations, with the same functional and basis set, were performed for all of the optimized structures to simulate the absorption spectra, where the first 100 excited states were calculated and a Gaussian line width of 0.08 eV was used to reproduce inhomogeneous broadening of absorption spectra. FRET rates were then calculated between different SiNC donor/acceptor pairs based on the transition density matrix, which goes beyond dipole−dipole coupling to include all multipole contributions. Details can be found in the Supporting Information. MC simulations for aggregates of noninteracting SiNCs were obtained by first generating *on*−*off* trajectories for individual SiNCs through an approach outlined in the Supporting Information. The simulation was specifically designed to mimic the measurements. Blinking traces for assemblies composed of *N* noninteracting SiNCs were then generated by adding *N* independent single SiNC spectra and rebinning to 0 and 1. Details are given in the Supporting Information.

Conflict of Interest: The authors declare no competing financial interest.

Acknowledgment. The authors thank Dmitri Kilin and Boris Shklovskii for fruitful discussions and comments. E.K.H. acknowledges the support of the National Science Foundation (NSF) through CBET-1133135 and U.S. Department of Energy (DOE) through DE-FG36-08GO88160. R.J.A. and U.R.K. acknowledge primary support through the NSF under MRSEC grant DMR-0819885 and DMR-1420013. K.A.V. was supported by the Center for Advanced Solar Photophysics, an Energy Frontier Research Center funded by the Office of Basic Energy Sciences, Office of Science, DOE. S.K. acknowledges financial support of the DOE Early Career Research grant DE-SC008446. For computational resources and administrative support, we thank the

Center for Computationally Assisted Science and Technology (CCAST) at North Dakota State University and the National Energy Research Scientific Computing Center (NERSC) allocation award 86678, supported by the Office of Science of the DOE under contract no. DE-AC02-05CH11231. Computational work was performed, in part, at the Center for Integrated Nanotechnologies (CINT), an Office of Science User Facility operated for the DOE Office of Science by Los Alamos National Laboratory (contract DE-AC52-06NA25396) and Sandia National Laboratories (contract DE-AC04-94AL85000).

Supporting Information Available: The Supporting Information is available free of charge on the ACS Publications website at DOI: 10.1021/acsnano.5b02676.

Movie 1, F-LP (40 μm width) (AVI)
Movie 2, F-HP (40 μm width) (AVI)
Details related to SiNC purification, experimental setup, cluster size determination, blinking statistics, MC simulations, and DFT calculations (PDF)

REFERENCES AND NOTES

1. Howes, P. D.; Chandrawati, R.; Stevens, M. M. Colloidal Nanoparticles as Advanced Biological Sensors. *Science* **2014**, *346*, 1247390.
2. Rakovich, T. Y.; Mahfoud, O. K.; Mohamed, B. M.; Prina-Mello, A.; Crosbie-Staunton, K.; Van den Broeck, T.; De Kimpe, L.; Sukhanova, A.; Baty, D.; Rakovich, A.; et al. Highly Sensitive Single Domain Antibody-Quantum Dot Conjugates for Detection of HER2 Biomarker in Lung and Breast Cancer Cells. *ACS Nano* **2014**, *8*, 5682–5695.
3. Bruchez, M.; Moronne, M.; Gin, P.; Weiss, S.; Alivisatos, A. P. Semiconductor Nanocrystals as Fluorescent Biological Labels. *Science* **1998**, *281*, 2013–2016.
4. Winnik, F. M.; Maysinger, D. Quantum Dot Cytotoxicity and Ways to Reduce It. *Acc. Chem. Res.* **2012**, *46*, 672–680.
5. Contreras, E. Q.; Cho, M.; Zhu, H.; Puppala, H. L.; Escalera, G.; Zhong, W.; Colvin, V. L. Toxicity of Quantum Dots and Cadmium Salt to Caenorhabditis Elegans after Multigenerational Exposure. *Environ. Sci. Technol.* **2012**, *47*, 1148–1154.
6. Qu, Y.; Li, W.; Zhou, Y.; Liu, X.; Zhang, L.; Wang, L.; Li, Y.-F.; Iida, A.; Tang, Z.; Zhao, Y.; et al. Full Assessment of Fate and Physiological Behavior of Quantum Dots Utilizing Caenorhabditis Elegans as a Model Organism. *Nano Lett.* **2011**, *11*, 3174–3183.
7. Mangolini, L. Synthesis, Properties, and Applications of Silicon Nanocrystals. *J. Vac. Sci. & Technol. B* **2013**, *31*, 020801.
8. Anthony, R. J.; Rowe, D. J.; Stein, M.; Yang, J.; Kortshagen, U. Routes to Achieving High Quantum Yield Luminescence from Gas-Phase-Produced Silicon Nanocrystals. *Adv. Funct. Mater.* **2011**, *21*, 4042–4046.
9. Pi, X. D.; Liptak, R. W.; Nowak, J. D.; Wells, N.; Carter, C. B.; Campbell, S.; Kortshagen, U. Air-Stable Full-Visible-Spectrum Emission from Silicon Nanocrystal Ensembles Synthesized by an All-Gas-Phase Plasma Approach. *Nanotechnology* **2008**, *19*, 245603.
10. Mangolini, L.; Kortshagen, U. Plasma-Assisted Synthesis of Silicon Nanocrystal Inks. *Adv. Mater.* **2007**, *19*, 2513–2519.
11. Jurbergs, D.; Rogojina, E.; Mangolini, L.; Kortshagen, U. Silicon Nanocrystals with Ensemble Quantum Yields Exceeding 60%. *Appl. Phys. Lett.* **2006**, *88*, 233116.
12. Hessel, C. M.; Reid, D.; Panthani, M. G.; Rasch, M. R.; Goodfellow, B. W.; Wei, J.; Fujii, H.; Akhavan, V.; Korgel, B. A. Synthesis of Ligand-Stabilized Silicon Nanocrystals with Size-Dependent Photoluminescence Spanning Visible to Near-Infrared Wavelengths. *Chem. Mater.* **2012**, *24*, 393–401.
13. Liu, S. M.; Yang, Y.; Sato, S.; Kimura, K. Enhanced Photoluminescence from Si Nano-Organosols by Functionalization with Alkenes and Their Size Evolution. *Chem. Mater.* **2006**, *18*, 637–642.
14. Zou, J.; Sanelle, P.; Pettigrew, K. A.; Kauzlarich, S. M. Size and Spectroscopy of Silicon Nanoparticles Prepared *via* Reduction of SiC_{14}. *J. Cluster Sci.* **2006**, *17*, 565–578.
15. Belomoin, G.; Therrien, J.; Nayfeh, M. Oxide and Hydrogen Capped Ultrasmall Blue Luminescent Si Nanoparticles. *Appl. Phys. Lett.* **2000**, *77*, 779–782.
16. Henderson, E. J.; Kelly, J. A.; Veinot, J. G. C. Influence of $HSiO_{1.5}$ Sol-Gel Polymer Structure and Composition on the Size and Luminescent Properties of Silicon Nanocrystals. *Chem. Mater.* **2009**, *21*, 5426–5434.
17. Mastronardi, M. L.; Maier-Flaig, F.; Faulkner, D.; Henderson, E. J.; Kübel, C.; Lemmer, U.; Ozin, G. A. Size-Dependent Absolute Quantum Yields for Size-Separated Colloidally-Stable Silicon Nanocrystals. *Nano Lett.* **2012**, *12*, 337–342.
18. Locritani, M.; Yu, Y.; Bergamini, G.; Baroncini, M.; Molloy, J. K.; Korgel, B. A.; Ceroni, P. Silicon Nanocrystals Functionalized with Pyrene Units: Efficient Light-Harvesting Antennae with Bright Near-Infrared Emission. *J. Phys. Chem. Lett.* **2014**, *5*, 3325–3329.
19. Sugimoto, H.; Fujii, M.; Imakita, K. Synthesis of Boron and Phosphorus Codoped All-Inorganic Colloidal Silicon Nanocrystals from Hydrogen Silsesquioxane. *Nanoscale* **2014**, *6*, 12354–12359.
20. Sugimoto, H.; Fujii, M.; Fukuda, Y.; Imakita, K.; Akamatsu, K. All-Inorganic Water-Dispersible Silicon Quantum Dots: Highly Efficient Near-Infrared Luminescence in a Wide pH Range. *Nanoscale* **2014**, *6*, 122–126.
21. Miller, J. B.; Van Sickle, A. R.; Anthony, R. J.; Kroll, D. M.; Kortshagen, U. R.; Hobbie, E. K. Ensemble Brightening and Enhanced Quantum yield in Size-Purified Silicon Nanocrystals. *ACS Nano* **2012**, *6*, 7389–7396.
22. Miller, J. B.; Harris, J. M.; Hobbie, E. K. Purifying Colloidal Nanoparticles through Ultracentrifugation with Implications for Interfaces and Materials. *Langmuir* **2014**, *30*, 7936–7946.
23. Miller, J. B.; Hobbie, E. K. Nanoparticles as Macromolecules. *J. Polym. Sci., Part B: Polym. Phys.* **2013**, *51*, 1195–1208.
24. Mastronardi, M. L.; Hennrich, F.; Henderson, E. J.; Maier-Flaig, F.; Blum, C.; Reichenbach, J.; Lemmer, U.; Kübel, C.; Wang, D.; Kappes, M. M.; et al. Preparation of Monodisperse Silicon Nanocrystals Using Density Gradient Ultracentrifugation. *J. Am. Chem. Soc.* **2011**, *133*, 11928–11931.
25. Erogbogbo, F.; Yong, K.-T.; Roy, I.; Xu, G.; Prasad, P. N.; Swihart, M. T. Biocompatible Luminescent Silicon Quantum Dots for Imaging of Cancer Cells. *ACS Nano* **2008**, *2*, 873–878.
26. Fujioka, K.; Hiruoka, M.; Sato, K.; Manabe, N.; Miyasaka, R.; Hanada, S.; Hoshino, A.; Tilley, R. D.; Manome, Y.; Hirakuri, K.; et al. Luminescent Passive-Oxidized Silicon Quantum Dots as Biological Staining Labels and Their Cytotoxicity Effects at High Concentration. *Nanotechnology* **2008**, *19*, 415102.
27. McVey, B. F. P.; Tilley, R. D. Solution Synthesis, Optical Properties and Bioimaging Applications of Silicon Nanocrystals. *Acc. Chem. Res.* **2014**, *47*, 3045–3051.
28. Sychugov, I.; Fucikova, A.; Pevere, F.; Yang, Z.; Veinot, J. G. C.; Linnros, J. Ultranarrow Luminescence Linewidth of Silicon Nanocrystals and Influence of Matrix. *ACS Photonics* **2014**, *1*, 998–1005.
29. Yang, Z.; Dasog, M.; Dobbie, A. R.; Lockwood, R.; Zhi, Y.; Meldrum, A.; Veinot, J. G. C. Highly Luminescent Covalently Linked Silicon Nanocrystal/Polystyrene Hybrid 26. Functional Materials: Synthesis, Properties, and Processability. *Adv. Funct. Mater.* **2014**, *24*, 1345–1353.
30. Van Sickle, A. R.; Miller, J. B.; Moore, C.; Anthony, R. J.; Kortshagen, U. R.; Hobbie, E. K. Temperature Dependent Photoluminescence of Size-Purified Silicon Nanocrystals. *ACS Appl. Mater. Interfaces* **2013**, *5*, 4233–4238.
31. Dohnalova, K.; Gregorkiewicz, T.; Kusova, K. Silicon Quantum Dots: Surface Matters. *J. Phys.: Condens. Matter* **2014**, *26*, 173201.
32. Dohnalová, K.; Poddubny, A. N.; Prokofiev, A. A.; de Boer, W. D. A. M.; Umesh, C. P.; Paulusse, J. M. J.; Zuilhof, H.; Gregorkiewicz, T. Surface Brightens up Si Quantum Dots: Direct Bandgap-Like Size-Tunable Emission. *Light: Sci. Appl.* **2013**, *2*, e47.

33. Kallel, H.; Arbouet, A.; Carrada, M.; Ben Assayag, G.; Chehaidar, A.; Periwal, P.; Baron, T.; Normand, P.; Paillard, V. Photoluminescence Enhancement of Silicon Nanocrystals Placed in the Near Field of a Silicon Nanowire. *Phys. Rev. B: Condens. Matter Mater. Phys.* **2013**, *88*, 081302.
34. Valenta, J.; Greben, M.; Gutsch, S.; Hiller, D.; Zacharias, M. Effects of Inter-Nanocrystal Distance on Luminescence Quantum Yield in Ensembles of Si Nanocrystals. *Appl. Phys. Lett.* **2014**, *105*, 243107.
35. Tice, D. B.; Frederick, M. T.; Chang, R. P. H.; Weiss, E. A. Electron Migration Limits the Rate of Photobrightening in Thin Films of CdSe Quantum Dots in a Dry N_2 (g) Atmosphere. *J. Phys. Chem. C* **2011**, *115*, 3654–3662.
36. Hua, Z.; Xu, Q. F.; Huang, X. N.; Zhang, C. F.; Wang, X. Y.; Xiao, M. Energy Transfer from a Single Semiconductor Nanocrystal to Dye Molecules. *ACS Nano* **2014**, *8*, 7060–7066.
37. Ajayi, O. A.; Anderson, N. C.; Cotlet, M.; Petrone, N.; Gu, T.; Wolcott, A.; Gesuele, F.; Hone, J.; Owen, J. S.; Wong, C. W. Time-Resolved Energy Transfer from Single Chloride-Terminated Nanocrystals to Graphene. *Appl. Phys. Lett.* **2014**, *104*, 171101.
38. Xu, Z.; Hine, C.; Maye, M.; Cotlet, M. Shell-Thickness Dependent Hole Transfer in Conjugated Polymer/Quantum Dot Hybrids. *ACS Nano* **2012**, *6*, 4984–4992.
39. Nguyen, H. M.; Seitz, O.; Peng, W. N.; Gartstein, Y. N.; Chabal, Y. J.; Malko, A. V. Efficient Radiative and Nonradiative Energy Transfer from Proximal CdSe/ZnS Nanocrystals into Silicon Nanomembranes. *ACS Nano* **2012**, *6*, 5574–5582.
40. Fernee, M. J.; Tamarat, P.; Lounis, B. Spectroscopy of Single Nanocrystals. *Chem. Soc. Rev.* **2014**, *43*, 1311–1337.
41. Vanmaekelbergh, D.; Casavola, M. Single-Dot Microscopy and Spectroscopy for Comprehensive Study of Colloidal Nanocrystals. *J. Phys. Chem. Lett.* **2011**, *2*, 2024–2031.
42. Galland, C.; Ghosh, Y.; Steinbruck, A.; Sykora, M.; Hollingsworth, J. A.; Klimov, V. I.; Htoon, H. Two Types of Luminescence Blinking Revealed by Spectroelectrochemistry of Single Quantum Dots. *Nature* **2011**, *479*, 203–207.
43. Pelton, M.; Smith, G.; Scherer, N. F.; Marcus, R. A. Evidence for a Diffusion-Controlled Mechanism for Fluorescence Blinking of Colloidal Quantum Dots. *Proc. Natl. Acad. Sci. U. S. A.* **2007**, *104*, 14249–14254.
44. Tang, J.; Marcus, R. A. Determination of Energetics and Kinetics from Single-Particle Intermittency and Ensemble-Averaged Fluorescence Intensity Decay of Quantum Dots. *J. Chem. Phys.* **2006**, *125*, 044703.
45. Durisic, N.; Wiseman, P. W.; Gruetter, P.; Heyes, C. D. A Common Mechanism Underlies the Dark Fraction Formation and Fluorescence Blinking of Quantum Dots. *ACS Nano* **2009**, *3*, 1167–1175.
46. Cichos, F.; von Borczyskowski, C.; Orrit, M. Power-Law Intermittency of Single Emitters. *Curr. Opin. Colloid Interface Sci.* **2007**, *12*, 272–284.
47. Schmidt, R.; Krasselt, C.; Goehler, C.; von Borczyskowski, C. The Fluorescence Intermittency for Quantum Dots Is Not Power-Law Distributed: A Luminescence Intensity Resolved Approach. *ACS Nano* **2014**, *8*, 3506–3521.
48. Bruhn, B.; Qejvanaj, F.; Gregorkiewicz, T.; Linnros, J. Temporal Correlation of Blinking Events in CdSe/ZnS and Si/SiO2 Nanocrystals. *Phys. B* **2014**, *453*, 63–67.
49. Hefti, R.; Jones, M.; Moyer, P. J. Long-Range Correlated Fluorescence Blinking in CdSe/ZnS Quantum Dots. *J. Phys. Chem. C* **2012**, *116*, 25617–25622.
50. Osborne, M. A.; Lees, S. F. Quantum Dot Photoluminescence Activation and Decay: Dark, Bright, and Reversible Populations in ZnS-Capped CdSe Nanocrystals. *ACS Nano* **2011**, *5*, 8295–8304.
51. Volkan-Kacso, S.; Frantsuzov, P. A.; Janko, B. Correlations between Subsequent Blinking Events in Single Quantum Dots. *Nano Lett.* **2010**, *10*, 2761–2765.
52. Goushi, K.; Yamada, T.; Otomo, A. Excitation Intensity Dependence of Power-Law Blinking Statistics in Nanocrystal Quantum Dots. *J. Phys. Chem. C* **2009**, *113*, 20161–20168.
53. Chung, I.; Witkoskie, J. B.; Cao, J. S.; Bawendi, M. G. Description of the Fluorescence Intensity Time Trace of Collections of CdSe Nanocrystal Quantum Dots based on Single Quantum Dot Fluorescence Blinking Statistics. *Phys, Rev. E* **2006**, *73*, 011106.
54. Tang, J.; Marcus, R. A. Mechanisms of Fluorescence Blinking in Semiconductor Nanocrystal Quantum Dots. *J. Chem. Phys.* **2005**, *123*, 054704.
55. Verberk, R.; Orrit, M. Photon Statistics in the Fluorescence of Single Molecules and Nanocrystals: Correlation Functions *versus* Distributions of On- and Off-Times. *J. Chem. Phys.* **2003**, *119*, 2214–2222.
56. Crouch, C. H.; Sauter, O.; Wu, X.; Purcell, R.; Querner, C.; Drndic, M.; Pelton, M. Facts and Artifacts in the Blinking Statistics of Semiconductor Nanocrystals. *Nano Lett.* **2010**, *10*, 1692–1698.
57. Amecke, A.; Heber, A.; Cichos, F. Distortion of Power Law Blinking with Binning and Thresholding. *J. Chem. Phys.* **2014**, *140*, 114306.
58. Houel, J.; Doan, Q. T.; Cajgfinger, T.; Ledoux, G.; Amans, D.; Aubret, A.; Dominjon, A.; Ferriol, S.; Barbier, R.; Nasilowski, M.; et al. Autocorrelation Analysis for the Unbiased Determination of Power-Law Exponents in Single-Quantum-Dot Blinking. *ACS Nano* **2015**, *9*, 886–893.
59. English, D. S.; Pell, L. E.; Yu, Z.; Barbara, P. F.; Korgel, B. A. Size Tunable Visible Luminescence from Individual Organic Monolayer Stabilized Silicon Nanocrystal Quantum Dots. *Nano Lett.* **2002**, *2*, 681–685.
60. Munro, A. M.; Ginger, D. S. Photoluminescence Quenching of Single CdSe Nanocrystals by Ligand Adsorption. *Nano Lett.* **2008**, *8*, 2585–2590.
61. Chizhik, A. I.; Schmidt, T.; Chizhik, A. M.; Huisken, F.; Meixner, A. J. Dynamical Effects of Defect Photoluminescence from Single SiO_2 and Si Nanoparticles. *Phys. Procedia* **2011**, *13*, 28–32.
62. Califano, M.; Gomez-Campos, F. M. Universal Trapping Mechanism in Semiconductor Nanocrystals. *Nano Lett.* **2013**, *13*, 2047–2052.
63. Mangum, B. D.; Wang, F.; Dennis, A. M.; Gao, Y. Q.; Ma, X. D.; Hollingsworth, J. A.; Htoon, H. Competition between Auger Recombination and Hot-Carrier Trapping in PL Intensity Fluctuations of Type II Nanocrystals. *Small* **2014**, *10*, 2892–2901.
64. Bell, D. M.; Howder, C. R.; Johnson, R. C.; Anderson, S. L. Single CdSe/ZnS Nanocrystals in an Ion Trap: Charge and Mass Determination and Photophysics Evolution with Changing Mass, Charge, and Temperature. *ACS Nano* **2014**, *8*, 2387–2398.
65. Tenne, R.; Teitelboim, A.; Rukenstein, P.; Dyshel, M.; Mokari, T.; Oron, D. Studying Quantum Dot Blinking through the Addition of an Engineered Inorganic Hole Trap. *ACS Nano* **2013**, *7*, 5084–5090.
66. Li, S.; Steigerwald, M. L.; Brus, L. E. Surface States in the Photoionization of High-Quality CdSe Core/Shell Nanocrystals. *ACS Nano* **2009**, *3*, 1267–1273.
67. Wang, X. Y.; Ren, X. F.; Kahen, K.; Hahn, M. A.; Rajeswaran, M.; Maccagnano-Zacher, S.; Silcox, J.; Cragg, G. E.; Efros, A. L.; Krauss, T. D. Non-Blinking Semiconductor Nanocrystals. *Nature* **2009**, *459*, 686–689.
68. Park, Y. S.; Bae, W. K.; Padilha, L. A.; Pietryga, J. M.; Klimov, V. I. Effect of the Core/Shell Interface on Auger Recombination Evaluated by Single-Quantum-Dot Spectroscopy. *Nano Lett.* **2014**, *14*, 396–402.
69. Zhang, A. D.; Dong, C. Q.; Liu, H.; Ren, J. C. Blinking Behavior of CdSe/CdS Quantum Dots Controlled by Alkylthiols as Surface Trap Modifiers. *J. Phys. Chem. C* **2013**, *117*, 24592–24600.
70. Early, K. T.; Nesbitt, D. J. Size-Dependent Photoionization in Single CdSe/ZnS Nanocrystals. *Nano Lett.* **2013**, *13*, 4844–4849.
71. Qin, W.; Guyot-Sionnest, P. Evidence for the Role of Holes in Blinking: Negative and Oxidized CdSe/CdS Dots. *ACS Nano* **2012**, *6*, 9125–9132.
72. Jin, S.; Song, N.; Lian, T. Suppressed Blinking Dynamics of Single QDs on ITO. *ACS Nano* **2010**, *4*, 1545–1552.

73. Velizhanin, K. A.; Piryatinski, A.; Chernyak, V. Y. Low-Temperature Hopping Dynamics with Energy Disorder: Renormalization Group Approach. *J. Chem. Phys.* **2013**, *139*, 084118.
74. Brawand, N. P.; Voros, M.; Galli, G. Surface Dangling Bonds are a Cause of B-Type Blinking in Si Nanoparticles. *Nanoscale* **2015**, *7*, 3737–3744.
75. Lin, Z.; Li, H.; Franceschetti, A.; Lusk, M. T. Efficient Exciton Transport between Strongly Quantum-Confined Silicon Quantum Dots. *ACS Nano* **2012**, *6*, 4029–4038.
76. Allan, G.; Delerue, C. Energy Transfer between Semiconductor Nanocrystals: Validity of Förster's Theory. *Phys. Rev. B: Condens. Matter Mater. Phys.* **2007**, *75*, 195311.
77. Bruhn, B.; Valenta, J.; Sangghaleh, F.; Linnros, J. Blinking Statistics of Silicon Quantum Dots. *Nano Lett.* **2011**, *11*, 5574–5580.
78. Valenta, J.; Fucikova, A.; Vacha, F.; Adamec, F.; Humpolickova, J.; Hof, M.; Pelant, I.; Kusova, K.; Dohnalova, K.; Linnros, J. Light-Emission Performance of Silicon Nanocrystals Deduced from Single Quantum Dot Spectroscopy. *Adv. Funct. Mater.* **2008**, *18*, 2666–2672.
79. Cichos, F.; Martin, J.; von Borczyskowski, C. Emission Intermittency in Silicon Nanocrystals. *Phys. Rev. B: Condens. Matter Mater. Phys.* **2004**, *70*, 115314.
80. Wintle, H. J. Decay of Static Electrification by Conduction Processes in Polyethylene. *J. Appl. Phys.* **1970**, *41*, 4004–4007.
81. Whitcomb, K. J.; Ryan, D. P.; Gelfand, M. P.; Van Orden, A. Blinking Statistics of Small Clusters of Semiconductor Nanocrystals. *J. Phys. Chem. C* **2013**, *117*, 25761–25768.
82. Wang, S. Y.; Querner, C.; Dadosh, T.; Crouch, C. H.; Novikov, D. S.; Drndic, M. Collective Fluorescence Enhancement in Nanoparticle Clusters. *Nat. Commun.* **2011**, *2*, 364.
83. Shepherd, D. P.; Whitcomb, K. J.; Milligan, K. K.; Goodwin, P. M.; Gelfand, M. P.; Van Orden, A. Fluorescence Intermittency and Energy Transfer in Small Clusters of Semiconductor Quantum Dots. *J. Phys. Chem. C* **2010**, *114*, 14831–14837.
84. Wang, S.; Querner, C.; Fischbein, M. D.; Willis, L.; Novikov, D. S.; Crouch, C. H.; Drndic, M. Blinking Statistics Correlated with Nanoparticle Number. *Nano Lett.* **2008**, *8*, 4020–4026.
85. Yu, M.; Van Orden, M. Enhanced Fluorescence Intermittency of CdSe-ZnS Quantum-Dot Clusters. *Phys. Rev. Lett.* **2006**, *97*, 237402.
86. Kowerko, D.; Schuster, J.; Amecke, N.; Abdel-Mottaleb, M.; Dobrawa, R.; Wurthner, F.; von Borczyskowski, C. FRET and Ligand Related Non-FRET Processes in Single Quantum Dot-Perylene Bisimide Assemblies. *Phys. Chem. Chem. Phys.* **2010**, *12*, 4112–4123.
87. Akselrod, G. M.; Prins, F.; Poulikakos, L. V.; Lee, E. M.; Weidman, M. C.; Mork, A. J.; Willard, A. P.; Bulović, V.; Tisdale, W. A. Subdiffusive Exciton Transport in Quantum Dot Solids. *Nano Lett.* **2014**, *14*, 3556–3562.